Reconstructing the recent failure chronology of a multistage landslide complex using cosmogenic isotope concentrations: St Catherine's Point, UK

Article (Accepted Version)

Reconstructing the recent failure chronology of a multistage landslide complex using cosmogenic isotope concentrations: St Catherine's Point, UK

John Barlow[1*], Roger Moore[1], and Delia M. Gheorghiu [2]

[1]*Department of Geography, University of Sussex, Brighton, BN1 9QJ, UK*

[2]*NERC Cosmogenic Isotope Analysis Facility, SUERC, East Kilbride, G75 OQF, UK*

**Corresponding Author – john.barlow@sussex.ac.uk*

ABSTRACT

The pre-existing multistage landslide complex at St Catherine's Point comprises a series of large rotational and translational failures that form the western section of the Isle of Wight Undercliff, UK. Cosmogenic beryllium and aluminum concentrations extracted from chert samples of the Upper Greensand are used to date the most recent sequential failure events. We use our understanding of the failure mechanics and landslide geomorphology to produce a cosmogenic exposure model that incorporates pre-failure topography into our shielding calculations. This method allowed us to date two successive landslides at the site using ^{10}Be, the most recent of which occurred ~1064 ± 348 (± 1 σ) ^{10}Be years ago, much more recently than was previously thought. An earlier failure event is dated at ~3471 ± 348 ^{10}Be years, supporting the hypothesis that the St Catherine's Point landslide complex was reactivated by relative sea-level rise at the end of the Holocene Climatic Optimum period.

Key Words: Landslides, Cosmogenic Dating, St Catherine's Point

1. INTRODUCTION

Deep-seated landslide complexes are found throughout the world (e.g. Crozier et al., 1995; Hutchinson and Bromhead, 2002; Kasai et al., 2009; Della Seta et al., 2013; Young 2015). Removal of mass through erosional processes, seismic shaking, and fluctuations in ground water

hydrology alter the stress environment to which geological materials are exposed, which can lead to rotational or translational failure across shear surfaces (Petley and Allison, 1997). In coastal environments, the continual removal of material through marine erosion can often result in multiple stages of failure through time (e.g. Hutchinson 1988; Rudkin 1990; Della Seta et al., 2013). An example of this from the UK is St Catherine's Point landslide complex which forms the westernmost part of the Isle of Wight Undercliff, a pre-existing landslide complex on the south coast of the Isle of Wight (Fig. 1). Measuring approximately 12 km in length and reaching up to 0.6 km from crest to toe, the Undercliff represents one of the largest urbanized landslide complexes in western Europe. The small towns of Ventnor, Bonchurch, St Lawrence and Niton with a total resident population of 6,000 are located along the Undercliff. (Lee and Moore 1991; Moore et al., 1995; McInnes 2007; Gillarduzzi et al., 2007; Moore et al., 2010).

The litho-stratigraphy of the Undercliff is composed of a sequence of sandstones and clays overlain by the Lower Chalk formation as shown in Table 1 (Palmer et al., 2007). The regional dip is to seaward at 1.5º to 2º (White, 1921). However, both the dip and the height of the strata relative to sea-level are influenced by the St Lawrence syncline, the axis of which runs through the centre of the Undercliff between St Lawrence and Ventnor (Chandler, 1984; Hutchinson and Bromhead, 2002). Slope stability along the Undercliff is controlled by shear surfaces in the weaker stratigraphic layers, most importantly in units 4a and 4b of the Gault Formation and units 2b and 2d of the Sandrock Formation (Moore et al., 2010; Moore et al., 2007; Hutchinson and Bromhead, 2002). Currently, the landslides within the complex exist in a state of dynamic metastable equilibrium with winter groundwater levels resulting in higher ground motions following periods of high effective stress (Gillarduzzi et al., 2007; Moore et al., 2010). The landslide complex is thought to have been activated by the erosion of the St

47 Catherine's Deep, a submerged palaeovalley running parallel to the Undercliff approximately 2.8
48 km offshore, in conjunction with changes in base level and marine erosion associated with sea-
49 level rise during interglacial periods (Chandler, 1984; Moore et al., 2007).
50 The geomorphology of St Catherine's Point has been thoroughly investigated (e.g.
51 Hutchinson et al., 1991; Hutchinson and Bromhead, 2002; Hutchinson et al., 2002; McInnes
52 2007) and is summarized here. Due to its location on the western limb of the St Lawrence
53 syncline, the base of the Gault Formation is roughly 53m above sea-level and the Sandrock is
54 roughly at sea-level (Fig. 2A). Shear surfaces within these strata control instability at the site
55 (Hutchinson et al., 1991). The ground model (Hutchinson et al., 1991) indicates a rapid
56 multistage failure resulting from marine erosion. The failure mechanics have created three major
57 morphological features illustrated in Figs. 1 and 2A; a seaward block composed of a sequence of
58 sandstones and Gault Formation that has been displaced southwards by ~100 m, a landward
59 block formed by rotational failure of the Upper Greensand and Lower Chalk formations, and a
60 rear scarp of Upper Greensand and Lower Chalk. To the south, a large debris apron protects the
61 landslide blocks from marine erosion. The borehole data used to construct the ground model is
62 also shown in Fig. 2A. These boreholes did not penetrate the entire stratigraphic sequence such
63 that there is some subjectivity in the model (Hutchinson et al., 1991). Repeat surveys of concrete
64 markers placed across the landslide complex indicate the seaward block to be moving south at up
65 to 25 mm/a (Hutchinson et al., 1991). This rate of motion is probably in response to on-going
66 marine erosion and toe unloading of the debris apron. Movement in the debris apron that fronts
67 the complex has been measured at 10-20 mm/a in proximity to the St Catherine's Point
68 lighthouse and is primarily attributed to translational and rotational displacement of the debris
69 apron (Hutchinson et al., 2002).

While this work has succeeded in developing an understanding of landslide morpho-dynamics at the site, the chronology of mass movement during the Holocene remains poorly constrained. Previous landslide dating at St Catherine's Point has relied on radiocarbon dating of woody material found within the stratigraphy of the debris apron (Preece, 1986; Hutchinson, 1987; Hutchinson et al., 1991; Hutchinson and Bromhead, 2002). The debris apron is composed of two layers of blocky landslide debris predominantly derived from Lower Chalk and Upper Greensand separated by a middle layer of soils and woody debris. Preece (1986), dated organic material taken from the middle layer at the cliff edge of the debris apron approximately 200 m to the west of the lighthouse (Fig. 1). The samples, neither of which were obtained from an in situ stump, were dated to 4490 ± 40 years and 3960 ± 50 ^{14}C years. The older sample was found within a thicker section of the soil layer and was higher in the stratigraphy indicating either ground deformation or a more complex depositional history. The younger sample was found in a deposit of compressed woody debris (Preece, 1986). Based on the radiocarbon dates and the stratigraphy of the debris apron, Hutchinson et al. (1991) interpreted a reactivation of the landslide during the Holocene in response to sea-level rise. During the Pleistocene, periglacial processes would have been in operation at the site and are likely to have deposited Chalk debris across the coastal slope (Hutchinson, 1987). Either wave action or seepage erosion and landsliding would have removed these deposits and eroded the base of what is now the seaward block. Landslides and solifluction deposited the lower portion of the debris apron and based on the radiocarbon dates this occurred prior to ~4500 ^{14}C years (Hutchinson and Bromhead, 2002). Following a period of inactivity during which a soil layer developed on the debris apron, a second major event occurred depositing the upper layer of the debris apron. Finally, the most recent failure event involving rotational and translational failure resulted in the seaward block

93 moving southward causing large scale deformation of the debris apron. Based on weak
94 archaeological evidence, Hutchinson and Bromhead (2002) suggested that this most recent
95 failure event occurred prior to the Iron Age (~800BC - 43AD).
96 In order to further constrain the chronology of ground instability at the St Catherine's
97 Point landslide complex, we use cosmogenic ^{26}Al and ^{10}Be from samples of chert in the Upper
98 Greensand formation. Establishing the exposure age of rock based on the concentration of
99 cosmogenic nuclides (CN) is a well-established method of geochronology (e.g. Lal, 1991; Gosse
100 and Phillips, 2001; Dunai, 2010) and the use of CN in landslide dating has proven successful
101 within the research literature. For example, Ballantyne and Stone (2004) made use of
102 cosmogenic ^{10}Be in sandstone to date the Beinn Alligin rock avalanche in north-western
103 Scotland. After scaling production rates for topographic shielding and altitude, samples obtained
104 from boulders at the centre of the deposition zone indicated an exposure age of 3950 ± 320 ^{10}Be
105 years. Ivy-Ochs et al. (2009) used a combination of cosmogenic ^{10}Be and ^{36}Cl to date scarps and
106 boulders from the Flims landslide complex in Switzerland. Their model addressed a complex
107 system, with snowfall and glacial processes adding uncertainty to the exposure model. Several
108 stages of instability in the La Clapière landslide complex in south-east France have also been
109 successfully dated using ^{10}Be on a series of scarps (Bigot-Cormier et al., 2005). These previous
110 uses of in situ cosmogenic dating methods on landslides have assumed sample shielding from
111 topographic obstacles to be constant. Such studies have typically involved dating a discrete
112 landslide event or have dated sequential failure events from the same source area but deposited
113 proximal to one another (e.g. Sturzenegger et al., 2014).
114 This research represents the first use of a reconstructed topography to modify topographic
115 shielding calculations and therefore improve estimates of CN production rate through time. The

methods outlined here are directly transferrable to any site where geomorphological events have altered the topography in such a way that pre-event reconstruction is possible. Establishing the past behaviour of geomorphic systems in this way is useful in understanding environmental forcing and in making predictions regarding future behaviour.

2. METHODS

At St Catherine's Point, the mechanism of failure and the bedrock geology are both amenable to cosmogenic dating. The geometry of the rotated block establishes the pre-failure shielding of the backscarp (Fig. 2), an assumption that often proves problematic in the cosmogenic dating of landslides (Dunai, 2010). We assume that the ~20 m of overlying material provided shielding from muogenic accumulation prior to failure. In the case of multistage failures, ground motion is causing topographic changes to both the source areas as well as to deposited material resulting in changes to topographic shielding during the exposure history of a sample. However, where the failure mechanics of the landslide is well constrained, such as at St Catherine's Point, this can be used to reconstruct the pre-failure topography based on current block geometries. This allows for the modification of topographic shielding effects such that multiple failure stages can be reconstructed. Concentrations of both ^{26}Al and ^{10}Be were measured from samples taken from chert beds located in the Upper Greensand as illustrated in Figs. 1 and 2. Samples taken from an exposure on the backscarp were used to date the most recent failure. Exposure of the relict backscarp on the south face of the landward block and large boulders sitting on top of the seaward block is thought to be contemporaneous and associated with a major landslide event involving material overlying the Gault Formation on the seaward block as illustrated in Fig. 2. Samples taken from both are used to date a previous failure stage.

2.1 Sample preparation

Samples were prepared at the NERC Cosmogenic Isotope Analysis Facility (CIAF) in the Scottish Universities Environmental Research Centre (SUERC). Quartz was separated from other minerals by mechanical (crushing, grinding, magnetic separation using a Frantz machine) and chemical (hexafluorosilicic acid treatment and repetitive hydrofluoric acid leaching) procedures. The quartz purity was assayed with ICP-OES. Quartz was dissolved in 40% HF and spiked with 220 µg ^{9}Be carrier. Natural Al content in the quartz was between 720-1142 ppm, therefore no Al spike was added to the samples.

^{10}Be and ^{26}Al were extracted and mixed BeO-Nb and AlO-Ag targets were prepared following procedures adapted from Kohl and Nishiizumi (1992). The ^{10}Be/^{9}Be and ^{27}Al/^{26}Al ratios were measured with the 5 MV NEC Pelletron accelerator mass spectrometer (AMS) at SUERC (Xu et al., 2010). AMS primary Standards NIST SRM4325 and PRIME Z92-0222, with ^{10}Be/^{9}Be nominal ratios of 2.79E^{-11}and 4.11E^{-11} ^{26}Al/^{27}Al respectively, were used for the measurements (Freeman et al., 2004). These ratios agree well with the secondary standards prepared by Nishiizumi et al. (2007). The ^{10}Be and ^{26}Al ratios were subsequently converted to nuclide concentrations in quartz. The processed blank ^{10}Be/^{9}Be ratio was between 26-65% of the sample ^{10}Be/^{9}Be ratios and was subtracted from the measured ratios; no blank correction was needed for ^{26}Al/^{27}Al ratios. Details of samples and the analytical data related to each of them are given in Table 2.

2.2 Exposure ages

The analytical data and the surface exposure ages for each sample are given in Table 3. The exposure ages were calculated using the Cronus-Earth online calculator v. 2.2 (http://hess.ess.washington.edu/). The ^{10}Be ages were calculated using a ^{10}Be half-life of 1.36 Ma and the SHLH spallation production rate of 4.39 ± 0.37 atoms g^{-1}-a^{-1} (Lm scaling) obtained from

age-constrained calibration measurements (Balco et al., 2008). The ^{26}Al half-life of 705 ka was used in the calculations (Nishiizumi, 2004). The calculated age uncertainties are expressed as 1 σ (Table 3). Corrections for sample thickness (4-6.9 cm) assume an exponential depth decrease of in situ production rate and an attenuation length of 160 g cm^{-2}.

2.3 Shielding

Topographic shielding was calculated by generating a series of azimuth and elevation measurements in order to define the sky view at each site (Dunne et al., 1999; Balco et al., 2008). Sample locations were used in conjunction with high-resolution digital elevation model (DEM) data to create the sky view. These data were augmented with field measurements for samples taken close to very steep slopes in order to address the limitations of DEM data in reproducing these features (e.g. Zhou and Liu, 2004). We altered our shielding calculations to account for the changes in the surface morphology due to landsliding at the site as indicated in Table 3. For samples taken from the relict scarp face on the landward block, the DEM data were amended by rotating the current morphology 15º around an axis running parallel to the base of slope as illustrated in Fig. 3A. In addition to the changes in topographic shielding, the change in cosmogenic dose due to elevation (Stone, 2000; Gosse and Stone, 2009) was assessed by increasing the elevation of the sample sites by 58 m to their pre-failure values. The changes this has on the sky view at the two sample sites on this feature are shown in Fig. 3B. As is evident, shielding due to the seaward block is no longer present and the steeper slopes cause greater shielding to the north. Changes to shielding on the seaward block were estimated by maintaining the elevation of the sample points and moving them 100 m in land. The exposure model assumes negligible surface erosion on the chert due to its high strength properties and insoluble nature. In

order to test this assumption, an analysis of $^{26}Al/^{10}Be$ vs ^{10}Be was undertaken (e.g. Lal, 1991; Gosse and Phillips, 2001; Dunai, 2010).

With regard to the exposure model proposed, down-slope displacement of the seaward block may have impacted upon the topographic shielding at the sampling sites. If post-event block motion is a function of apron erosion, this suggests such rates would have been lower in the past. The current geometry is such that the highest inclination angle to the horizon is ~32°. Given that topographic shielding at this inclination angle is minimal, resultant changes to production rates due to small scale movement within the blocks is unlikely to be a significant source of experimental error and this is not considered in our exposure model (e.g. Dunne et al., 1999).

3. RESULTS AND DISCUSSION

Parameters and results of the cosmogenic dating are shown in Tables 2 and 3. Sample testing indicated high natural concentrations of ^{27}Al (720-1142 ppm) such that ^{26}Al results are considered unreliable (Dunai, 2010). An indication of this can be seen in the $^{10}Be/^{26}Al$ ratio in table 2. Theoretically, this should be 6.75 for samples that have experienced minimal erosion. However, all but two of our samples are higher than this value and one is significantly lower. To further evaluate this relationship, a plot of $^{26}Al/^{10}Be$ vs ^{10}Be is shown in Fig. 4. The plot indicates the erosional history of a sample where measured concentrations for the differing samples can be compared to theoretical concentrations based on the production ratio, the isotope half-life, and burial history (Lal, 1991; Gosse and Phillips, 2001). Samples with a simple burial history should plot between the upper two curves which has been termed the “steady-state erosion island” (Lal, 1991). The uppermost of these curves represents steady-state erosion for a sample that has never been buried and the curve plotting blow this represents a surface exposure evolving with zero

erosion. From left to right the steady–state curve plots decreasing erosion rates while the zero erosion curve plots increasing exposure duration (Dunai, 2010). Samples that plot above the steady-state erosion island are theoretically impossible and indicate either sample contamination or a measurement error while those that plot below indicate burial of the sample (Gosse and Phillips, 2001). Half of our samples plot within 1σ of the zero erosion curve (Fig. 4). Of the three that do not meet this criterion, SCARP2 and SB2 plot above the steady-state erosion island and are therefore considered to reflect measurement errors as a consequence of the high natural ^{27}Al content. Sample LB2 is indicative of rapid burial for ~1.5 Ma which is not possible at this site. This sample is interpreted as having a complex exposure history and is therefore not used in our exposure model. Discounting these three samples, the ^{26}Al data indicate the most recent failure occurred 1243 ± 395 (± 1 σ) ^{26}Al years ago. The mean estimate of the samples from the landward and seaward blocks indicates the previous failure occurred 3761 ± 464 ^{26}Al years ago.

As a consequence of the uncertainty around the ^{26}Al results, our interpretation relies solely on ^{10}Be data. Based on the samples from the backscarp, the most recent failure at the site is dated to 1064 ± 348 ^{10}Be years. Dating of the Upper Greensand blocks falls within 1 σ of the exposure age of the relict scarp face on the landward block confirming these blocks were deposited at the same time as the exposure of this feature. This suggests that the boulders were deposited along the top of the seaward block during the same event that exposed the relict scarp face at 3471 ± 366 ^{10}Be years. The upper layer of the debris apron would also have been deposited from this event. The boulders on top of the seaward block would then have been entrained when it moved down slope during the most recent failure dated at 1064 ± 348 ^{10}Be years. This sequence of events is in agreement with that suggested by Hutchinson et al. (1991) and is shown graphically in Fig. 2. The main source of error with ^{10}Be in diagenetic silica (chert)

is meteoric contamination of the samples (Zerathe et al., 2013). However, given the broad agreement of our results with usable ^{26}Al data and the radiocarbon dates reported by Preece (1986) it is unlikely that this is a significant source of error.

The data indicate a failure chronology for the St Catherine's Point landslide complex in relation to the Holocene transgression as illustrated in Fig. 5. Our data support the sequence of events given by Hutchinson et al. (1991) and Hutchinson and Bromhead (2002) although the most recent failure is much younger than was previously estimated. Relative sea-level rise associated with the Holocene Transgression stabilized between 7500 and 5000 years BP as illustrated in Fig. 5 (Shennan and Horton, 2002). Based on tidal data from the gauge at Sandown Pier (13.3 km NE), maximum tide height is +2.54 m above ordinance datum. Tidal water would therefore have been within reach of current mean sea-level ~ 5000 years ago. With regard to radiocarbon dating reported by Preece (1986), the sample dated to 3960 ± 50 ^{14}C years is roughly in agreement with our results for the major landsliding event forming the relict backscarp. The sample dated 4490 ± 40 ^{14}C years is more difficult to interpret. The main problem with using the dates of deposited woody debris to reconstruct landslide activity is the assumption that tree death is contemporaneous with landsliding and deposition which may not be the case with this sample. The study area would have been undergoing significant changes during the mid-Holocene due to both ground instability and sea-level rise. The age of this sample can be linked to the inundation of the near shore due to sea-level rise and an examination of the Mollusca present within the soil column at the sea cliff indicates a shaded environment (Preece,1986). It is therefore likely that the coastal slope was forested prior to inundation by rising sea-levels and landsliding in the mid Holocene. This tree was likely felled due to the previous landslide stage forming the lower strata

252 of the debris apron or sea water inundation. However, the sample suggests that the lower
253 landslide deposits of the debris apron were in place prior to 4490 ± 40 ^{14}C years ago.
254 Based on the timing of relative sea-level rise and the radiocarbon data provided by Preece
255 (1986), it is likely that initial reactivation of the landslide complex at St Catherine's point
256 occurred between ~5000 and ~4500 years ago. Following this initial failure, we date the next
257 event at 3471 ± 366 ^{10}Be years based on the exposure ages of the relict scarp face on the
258 landward block and the boulders located on top of the seaward block. The data therefore suggest
259 that the period immediately following the resumption of marine erosion at the site was very
260 active with two major events within ~1500 years. The debris apron would then have acted to
261 protect the site from marine erosion, with ~2500 years passing before the most recent failure
262 (Fig. 5).
263 **4. CONCLUSIONS**
264 Our results indicate that the current morphology of St Catherine's Point was formed by a
265 landslide event 1064 ±348 ^{10}Be years ago. This was the most recent of at least two major
266 landslide events which have occurred at the site since sea-levels stabilized in the mid-Holocene.
267 We date a previous event to 3471 ± 366 ^{10}Be years, or roughly 1500 years after sea-level
268 stabilization. Radiocarbon dating of a tree log in the debris apron (Preece, 1986) and the
269 stratigraphy of the debris apron suggests there may have been another major failure at the site
270 immediately following the stabilization of relative sea-level 5000 years ago. Based on these
271 results, the system shows high sensitivity to marine erosion. However, landslide deposits such as
272 the debris apron act as a negative feedback to this process as they both defend the base of slope
273 from erosion and provide confining stress to the blocks. Erosion of the debris apron is therefore
274 identified as a major trigger for landsliding at the site. Management decisions pertaining to slope

instability along the Isle of Wight Undercliff and the ~6000 people that dwell upon it requires accurate information about the past behaviour of the complex (Hutchinson et al., 1991). Our data indicate a strong empirical relationship between sea-level and past major landslide events at the site. Over the next century, the south coast of the Isle of Wight is predicted to experience sea-level rise of between 20 and 84 cm and extreme sea-level events are predicted to be 10 to 20 times more frequent (Moore et al., 2010). The resulting increases to erosion and toe unloading of the debris apron represents a significant potential trigger for future instability at St Catherine's Point and elsewhere in the Undercliff.

5. ACKNOWLEDGMENTS

This research was supported by the Natural Environment Research Council [CIAF # 9133-0413]. Measurement of samples (AMS) was undertaken by Dylan Rood. Digital data used in the analysis was provided courtesy of the Channel Coastal Observatory. The permission of the National Trust to access and recover the samples is gratefully acknowledged. We also wish to thank Andrew Plater, Vincent Regard and an anonymous reviewer for their helpful comments.

REFERENCES CITED

Balco, G., Stone, J.O., Lifton, N.A., Dunai, T.J., 2008. A complete and easily accessible means of calculating surface exposure ages or erosion rates from ^{10}Be and ^{26}Al measurements. Quaternary Geochronology. 3, 174-195.

Ballantyne, C., Stone, J.O., 2004. The Beinn Alligin rock Avalanche, NW Scotland: cosmogenic ^{10}Be dating, interpretation and significance. The Holocene. 14, 3, 448-453.

Bigot-Cormier, F., Braucher, R., Bourles, D., Guglielmi, Y., Dubar, M., Stephan, J.F., 2005. Chronological constraints on processes leading to large active landslides. Earth and Planetary Science Letters. 235, 141-150.

298 Chandler, M.P., 1984. The coastal landslides forming the Undercliff of the Isle of Wight. PhD
299 Thesis, Department of civil Engineering, Imperial College, University of London.
300 Crozier, M.J., Deimel, M.S., Simon, J.S, 1995. Investigation of earthquake triggering for deep-
301 seated landslides, Taranaki, New Zealand. Quaternary International, 25, 65-73.
302 Della Seta, M., Martino, S., Scarascia Mugnozza, G., 2013. Quaternary sea-level change and
303 slope instability in coastal areas: insights from the Vasto Landslide (Adriatic coast, central
304 Italy). Geomorphology, 201, 462–478
305 Dunai, T.J., 2010. Cosmogenic Nuclides Principles, Concepts and Applications in the Earth
306 Surface Sciences, Cambridge University Press, Cambridge.
307 Dunne, J., Elmore, D., Muzikar, P., 1999. Scaling factors for the rates of production of
308 cosmogenic nuclides for geometric shielding and attenuation at depth on sloped surfaces.
309 Geomorphology. 27, 3-11.
310 Freeman, S.P.H.T., Bishop, P., Bryant, C., Cook, G., Fallick, A., Harkness, D., Metcalfe, S.,
311 Scott, M., Scott, R., Summerfield, M., 2004. A new environmental sciences AMS
312 laboratory in Scotland. Nuclear Instruments and Methods in Physics Research B. 31, 223–
313 224, DOI: 10.1016/j.nimb.2004.04.010.
314 Gillarduzzi, A., Clark, A.R., Fort, D.S., Houghton J.E.M., 2007. Monitoring coastal slope
315 instability within the western Undercliff landslide, Isle of Wight, UK. In: McInnes, R.G.,
316 Jakeways, J., Fairbank, H., and Mathie, E., (Eds.) Landslides and Climate Change, Taylor
317 Frances, London; pp 345-354.
318 Gosse, J.C., Phillips, F.M., 2001. Terrestrial in situ cosmogenic nuclides: theory and application.
319 Quaternary Science Reviews. 20, 1475-1560.

320 Gosse, J.C., Stone, J.O., 2009. Terrestrial cosmogenic nuclide methods passing milestones
321 toward paleo-altimetry. EOS Transactions American Geophysical Union. 82, 82-89.
322 Hutchinson, J.N., 1987. Some coastal landslides of the southern Isle of Wight. In: Barber, K.E.,
323 (Ed.) Wessex and the Isle of Wight. Field Guide, Quaternary Research Association,
324 Cambridge, pp 123-135.
325 Hutchinson, J.N., 1988. General report. Morphological and geotechnical parameters of landslides
326 in relation to geology and hydrogeology. Proceedings of the 5th International Sympiosium
327 on Landslides, Lausanne, 1, 3-35.
328 Hutchinson, J.N., Bromhead, E.N., Chandler, M.P., 1991. Investigations of Landslides at St
329 Catherine's Point, Isle of Wight, In: Slope Stability Engineering: Developments and
330 Applications, Thomas Telford: London; pp.169-179.
331 Hutchinson, J.N., Bromhead, E.N., 2002. Keynote Paper: Isle of Wight landslides. In: McInnes,
332 R.G., Jakeways, J., (Eds.) Instability Planning and Management: Seeking Sustainable
333 Solutions to Ground Movement Problems, Proceedings of International Conference,
334 Ventnor. Thomas Telford, London, pp.3–70.
335 Hutchinson, J.N., Bromhead, E.N., Chandler, M.P., 2002. Landslide movements affecting the
336 lighthouse at Saint Catherine's Point, Isle of Wight. In: McInnes, R.G., Jakeways, J., (Eds.)
337 Instability Planning and Management: Seeking Sustainable Solutions to Ground Movement
338 Problems, Proceedings of International Conference, Ventnor. Thomas Telford, London,
339 pp.291-298.
340 Ivy-Ochs, S., Poschinger, A., Synal, H-A., Maisch, M., 2009. Surface exposure dating of the
341 Flims landslide, Graubünden, Switzerland. Geomorphology. 103, 104-112.

342 Kasai, M., Ikeda, M., Asahina, T., Fujisawa, K., 2009. LiDAR-derived DEM evaluation of deep-
343 seated landslides in a steep and rocky region of Japan. Geomorphology. 113, 57-69.
344 DOI:10.1016/j.geomorph.2009.06.004
345 Kohl, C., Nishiizumi, K., 1992. Chemical isolation of quartz for measurement of in situ-
346 produced cosmogenic nuclides. Geochi-mica et Cosmochimica Acta. 56, 3586–3587.
347 Lal, D., 1991. Cosmic ray labelling of erosion surfaces: in situ nuclide production rates and
348 erosion models. Earth and Planetary Science Letters. 104, 424-439.
349 Lee, E.M., Moore, R., 1991. Coastal Landslip Potential Assessment, Isle of Wight Undercliff,
350 Ventnor. Technical Report prepared by Geomorphological Services Ltd for the Department
351 of the Environment, research contract PECD 7/1/272.
352 Lee, E.M., Moore, R., 2007. Ventnor Undercliff: development of landslide scenarios and
353 quantitative risk assessment. Proceedings of the International Conference on Landslides
354 and Climate Change, Ventnor, Isle of Wight. pp. 323-333.
355 McInnes, R.G., 2007. The Undercliff of the Isle of Wight: a guide to managing ground
356 instability. Centre for the Coastal Environment, Isle of Wight Council, Report
357 CCN/ENV58.
358 Moore, R., Lee, E.M., Clark, A.R., 1995. The Undercliff of the Isle of Wight: a review of ground
359 behaviour. Cross Publishing. pp 68.
360 Moore, R., Carey, J.M., McInnes, R.G., 2010. Landslide behaviour and climate change:
361 predictable consequences for the Ventnor Undercliff, Isle of Wight. Quarterly Journal of
362 Engineering Geology and Hydrogeology. 43, 447-460.
363 Moore, R., Turner, M.D., Palmer, M.J., Carey, J.M., 2007. The Ventnor Undercliff: Landslide
364 model, mechanisms and causes, and the implications of climate change induced ground

behavior and risk. In: McInnes, R.G., Jakeways, J., Fairbank, H., Mathie, E., (Eds.) Landslides and Climate Change, Taylor Frances: London, pp 365-375.

Nishiizumi, K., Imamura, M., Caffee, M., Southon, J., Finkel, R., McAnich, J., 2007. Absolute calibration of ^{10}Be AMS standards. Nuclear Instruments and Methods in Physics Research. B 258, 403413.

Petley, D.N., Allison, R.J., 1997. The mechanics of deep-seated landslides. Earth Surface Processes and Landforms. 22, 747-758.

Preece, R.C., 1986. Faunal Remains from Radiocarbon-dated Soils within Landslip Debris from the Undercliff, Isle of Wight, Southern England. Journal of Archaeological Science, 13, 189-200.

Rudkin H.L., 1990. Stonebarrow Hill. In: Allison R.J. (Ed.) Landslides of the Dorset Coast. British Geomorphological Research Group Field Guide. Pp 87-93.

Shennan, I., Horton, B., 2002. Holocene land- and sea-level changes in Great Britain. Journal of Quaternary Science. 17, 5-6, 511-526.

Stone, J.O., 2000. Air pressure and cosmogenic isotope production. Journal of Geophysical Research. 105, B10, 23753-23759.

Sturzenegger, M., Stead, D., Gosse, J., Ward, B., Froese C., 2014. Reconstruction of the history of the Palliser Rockslide based on ^{36}Cl terrestrial cosmogenic nuclide dating and volume estimations. Landslides. DOI: 10.1007/s10346-014-0527-4.

White, H.J.O., 1921. A short account of the geology of the Isle of Wight. Memoir of the Geological Survey of England and Wales. HMSO, London.

Xu, S., Dougans, A.B., Freeman, S.P.H.T., Schnabel, C., Wilcken, K.M., 2010. Improved Be-10 and Al-26 AMS with a 5 MV spectrometer. Nuclear Instruments and Methods, B 268, 736–738

Young, A.P., 2015. Recent deep-seated coastal landsliding at San Onofre State Beach, California. Geomorphology. 228, 200-212. DOI: 10.1016/j.geomorph.2014.08.005

Zerathe, S., Braucher, R., Lebourg, T., Bourlès, D., Manetti, M., Léanni, L., 2013. Dating chert (diagenetic silica) using in-situ produced ^{10}Be: Possible complications revealed through a comparison with ^{36}Cl applied to coexisting limestone. Quaternary Geochronology, 17, 81-93, DOI: 10.1016/j.quageo.2013.01.003.

Zhou, Q., Liu, X., 2004. Analysis of errors of derived slope and aspect related to DEM data properties. Computers and Geosciences. 30, 369-378.

399

400 Table 1: Litho-stratigraphy of the Isle of Wight Undercliff at Ventnor (Palmer et al., 2007).

Stage	Formation	Unit	~ Thickness (m)
Cenomanian	Lower Chalk	6b	15-31.4
		6a	3.1-3.4
Upper Albion	Upper Greensand	5c	6-8
		5b	20.5-22
		5a	2.1-6.3
	Gault	4b	36-42
Lower Albion		4a	3.1-8.5
	Carstone	3	4.1-9.2
	Sandrock	2e	8.5-10.1
		2d	2.3-2.6
		2c	20.0-21.3
Upper Aptian		2b	8.3-9.3
		2a	3.6-4.6
Lower Aptian	Ferruginous Sands	1c	>11.4

Table 2: Sample locations and details - Items in brackets indicate parameters prior to the most recent landslide event.

Sample	Latitude (°N)	Longitude (°W)	Altitude (m)	Thickness (cm)	Density (g cm^{-3})	Shielding * (factor)
SCARP1	50.5811	-1.301	142	4.4	2.65	0.668
SCARP2	50.5811	-1.301	142	4.0	2.65	0.807
LB1	50.5798	-1.3017	86 (142)	5.6	2.65	0.976 (0.884)
LB2	50.5798	-1.3017	85 (141)	6.0	2.65	0.898 (0.843)
SB1	50.5793	-1.30	95 (95)	9.9	2.65	0.967 (0.967)
SB2	50.5793	-1.30	95 (95)	6.9	2.65	0.979 (0.965)

* Shielding computed after Dunne et al. (1999) and Balco et al. (2008).

Table 3: Analytical details and exposure ages of the sampled surfaces

Sample	^{10}Be atoms/g *	^{10}Be years **	^{26}Al atoms/g	^{26}Al years ***	Al/Be
SCARP1	4025±1961	1147±559(568)	30188±3163	1243±395(410)	7.5 ± 1.61
SCARP2	4259±1838	1011±436(445)	68151±6534	2357±529(567)	16.00 ± 3.55
LB1	12259±2976	2700±656(697)	116687±17395	3743±751(819)	9.52 ± 5.84
LB2	18847±4529	4364±1050(1116)	66854±8798	2269±522(558)	3.55 ± 1.94
SB1	18575±2646	4068±580(679)	117178±10998	3773±591(676)	6.31 ± 4.16
SB2	15248±3011	3268±646(706)	115863±15189	3608±698(765)	7.60 ± 5.04

* ^{10}Be concentrations. ^{10}Be/^{9}Be ratios measured against NIST SRM 4325 with nominal value of 2.79x10-11. ^{10}Be/^{9}Be ratios were corrected by a full chemistry procedural blank that yielded 26-65% of the number of ^{10}Be atoms in the samples;

** Exposure ages calculated using Cronus-Earth ^{10}Be – ^{26}Al exposure age calculator v. 2.2 (http://hess.ess.washington.edu/). They assume zero erosion, scaling factors according to Stone (2000) and a spallation production rate of 4.49 ± 0.39 atom (g SiO_2)$^{-1}$ a^{-1} (Balco et al., 2008). Exposure ages are presented with the internal uncertainties (external uncertainties in brackets).

*** ^{26}Al/^{27}Al ratios measured against PRIME-Z92-0222 with nominal value of 4.11E-11. No blank correction was needed for ^{26}Al/^{27}Al ratios.

Fig. 1. Site location. Shaded relief map of the Isle of Wight Undercliff and St Catherine's Point provided at larger scales with main geomorphological features and sampling sites indicated. Dashed line indicates cross sectional transect (Fig. 2). Topographic data courtesy of the Channel Coastal Observatory.

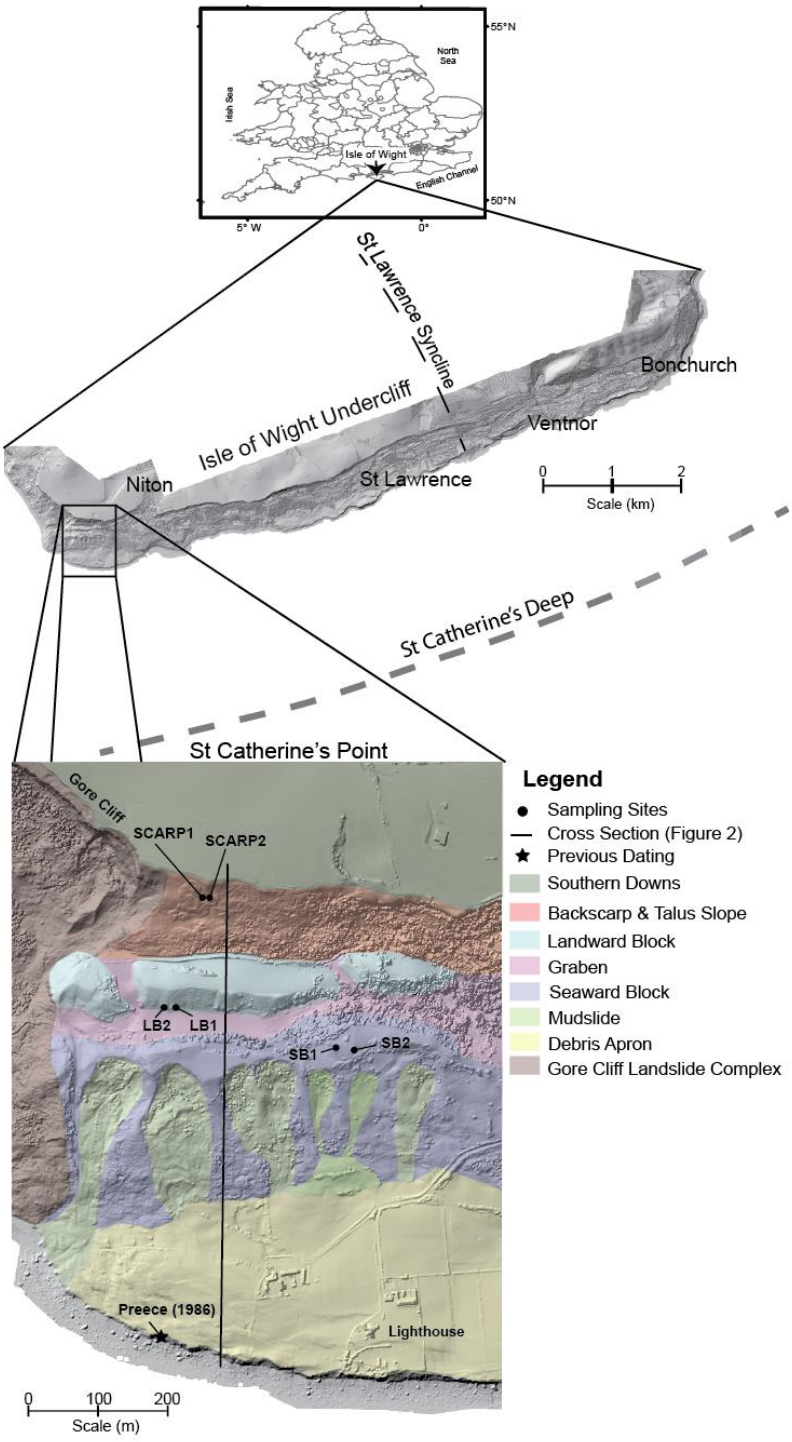

Fig. 2. Cross-sectional diagram showing the failure chronology of St Catherine's Point landslide complex. A) Current geomorphology. (after Hutchinson et al, 1991); B) Intermediary

geomorphology dated from 3471 -1064 ^{10}Be years; C) Geomorphology prior to failure dated at ~3471 ^{10}Be years.

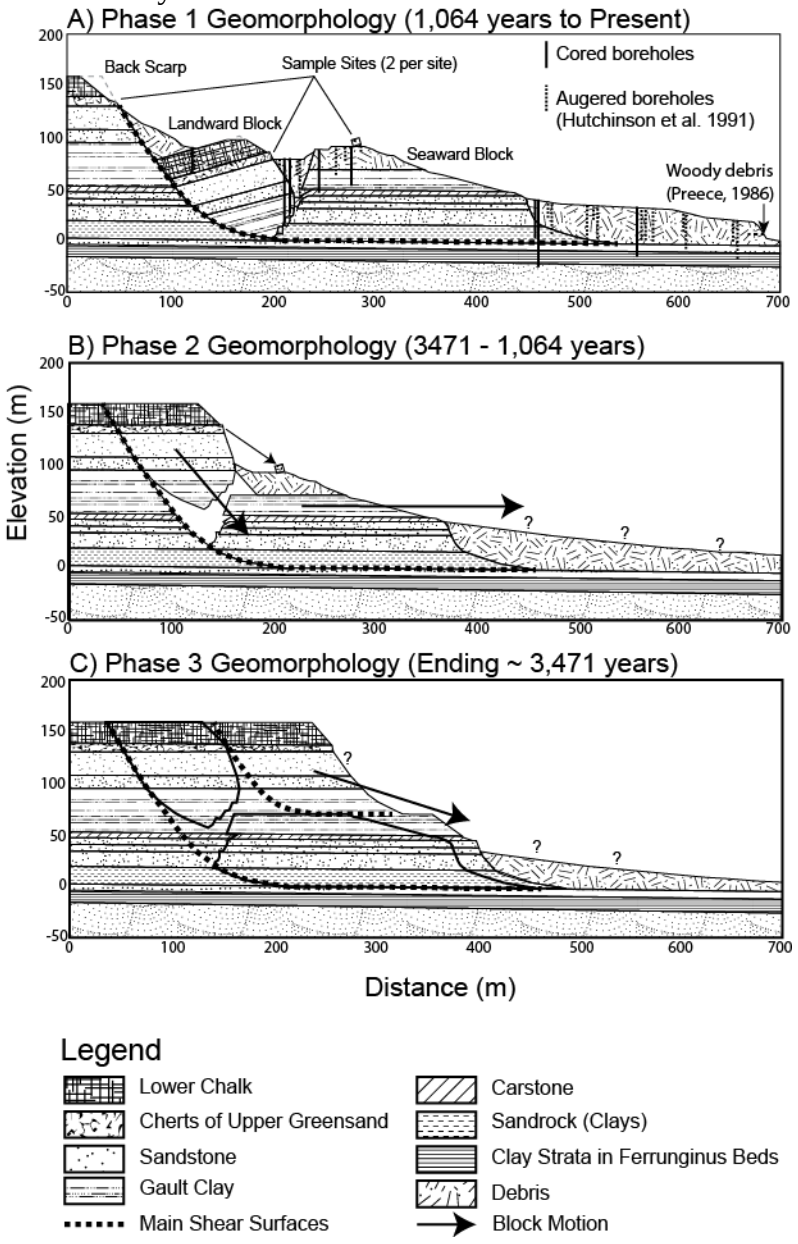

Fig. 3: Topographic shielding effects of rotating the landward block 15º. A) Graphic showing block morphology pre- and post-failure. B) Changes in sky view resulting from the rotation and elevation of the block. Black line indicates current sky view, grey line indicates pre-failure sky view.

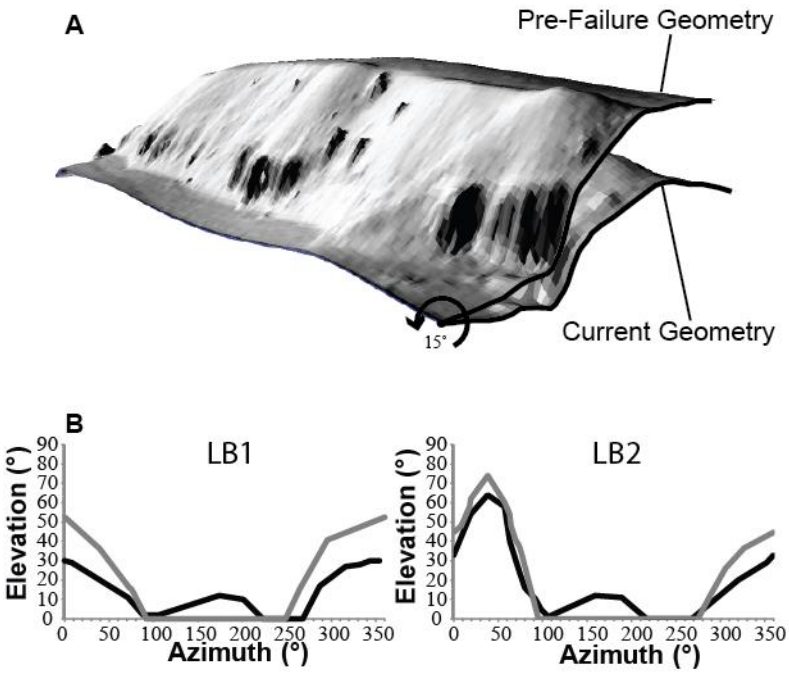

Fig. 4: Plot of $^{26}Al/^{10}Be$ vs. ^{10}Be. Black line indicates the zero erosion curve. Error ellipses indicate 1 σ.

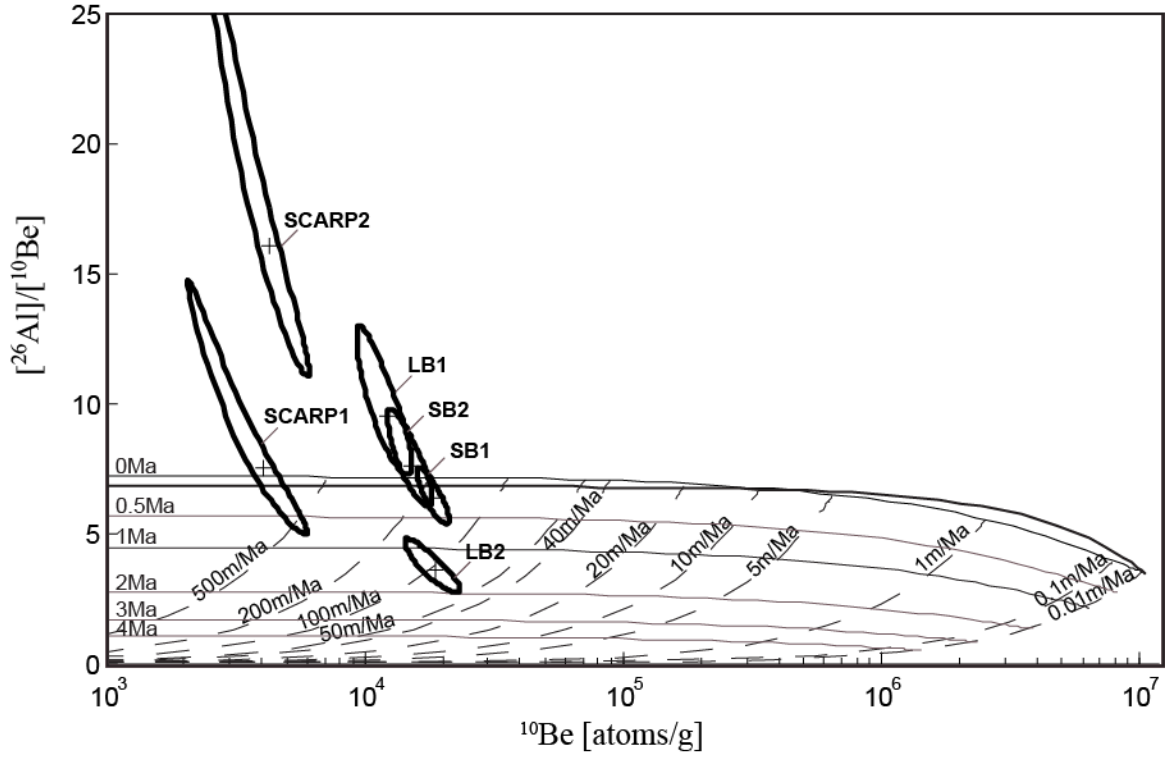

445 Fig. 5. Failure chronology of the St Catherine's Point landslide complex plotted with change in
446 relative sea-level during the Holocene. Error bars indicate 1 σ. Sea-level curve after Shennan and
447 Horton (2002).

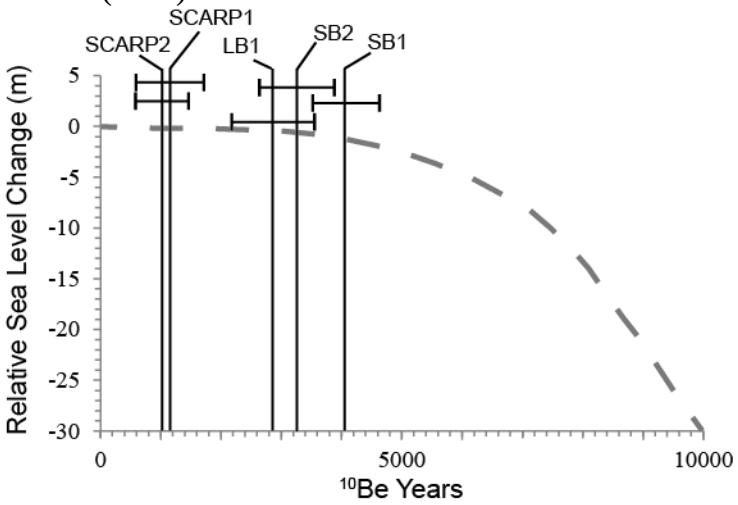

448
449

450